Thesis

On

DESIGN OF ALUMINIUM BASED ALLOY (Al6063) ULTRA-FINE GRAINED STRIPS USING HYBRID LSEM PROCESS

Submitted in partial fulfillment of the requirement for the award of the degree of

Master of Engineering

IN

PRODUCTION ENGINEERING

Submitted By

MAYUR SHARMA

Roll No.: 801482015

Under the guidance of

Dr. V.K SINGLA

Associate Professor

Mechanical Engineering Department

Thapar University, Patiala

DEPARTMENT OF MECHANICAL ENGINEERING

THAPAR UNIVERSITY

PATIALA-147004, INDIA

JULY 2016

DECLARATION

I hereby declare that this thesis entitled "**DESIGN OF ALUMINIUM BASED ALLOY (Al6063) ULTRA-FINE GRAINED STRIPS USING HYBRIS LSEM PROCESS**" is an authentic record of my study carried out as requirements for the award of the degree of **Masters of Engineering** in **Production Engineering** at **Thapar University, Patiala,** under the guidance of **Dr. V.K. Singla**, Associate Professor, Department of Mechanical Engineering, Thapar University, Patiala during July 2015 to July 2016. The matter embodied in this thesis report has not been submitted in part full to any other university or institute for award of any degree.

Date: 14/07/2016
Sharma

mayur sharma
Mayur

It is certified that the above statement made by the student is correct to best of my knowledge and belief.

14/7/2016
(Dr. V.K. SINGLA)

Associate Professor

Department of Mechanical Engineering,

Thapar University, Patiala- 147004

Countersigned By:

(Dr. S.K. MOHAPATRA)

Dean and Head

Mechanical Engineering Department

Thapar University, Patiala- 147004

(Dr. S.S. BHATIA)

Dean of Academic Affairs

Thapar University, Patiala- 147004

ACKNOWLEDGEMENT

I would like to express my gratitude to my guide **Dr. V.K Singla**, Associate Professor, Mechanical Engineering department, Thapar University, Patiala whose contribution in stimulating suggestions and encouragement, helped me to coordinate my thesis. I thank them for their continuous suggestions and help.

Furthermore I would also like to acknowledge the crucial role of the staff of Mechanical Engineering Department for their direct and indirect help in my thesis work.

I am also thankful to my friends for supporting me and continuously encouraging me during the period of work.

Mayur sharma

Mayur Sharma

ACKNOWLEDGEMENT

I would like to express my gratitude to my guide **Dr. V.K Singla**, Associate Professor, Mechanical Engineering department, Thapar University, Patiala whose contribution in stimulating suggestions and encouragement, helped me to coordinate my thesis. I thank them for their continuous suggestions and help.

Furthermore I would also like to acknowledge the crucial role of the staff of Mechanical Engineering Department for their direct and indirect help in my thesis work.

I am also thankful to my friends for supporting me and continuously encouraging me during the period of work.

Mayur Sharma

ABSTRACT

The present study focuses on formation of ultra-fine grained strips of controlled dimensions from Aluminium based alloy (Al6063) by Hybrid Extrusion–Machining process. This process has emerged as an alternate process for producing sheets, foils and plates from different variety of light weight alloys with properties superior to that of their counter-part. Hardness analysis of bulk and fabricated strips were conducted at both micro and nano level. The deformation analysis of the strips was done using X-Ray diffraction (XRD). Microstructural analysis was done by Electron back-scatter diffraction. Effect of different machining conditions on the surface roughness has also been studied. The result illustrates a significant increase in the hardness of the fabricated strips as consequence of reduced grain size. Influence of strain hardening on fabricability of strips has also been studied. Mechanical properties of fabricated strips and bulk Al6063 alloy at nano level were somewhat different from that of micro level.

ABBREVIATIONS

SPD	Severe plastic deformation
LSEM	Large strain extrusion machining
HSS	High speed steel
EDM	Electric discharge machining
FEM	Finite element method
Al	Aluminium
Mg	Magnesium
PDZ	Primary deformation zone
EBSD	Electron Backscatter Diffraction
α	Rake angle
γ	Shear strain
λ	Chip reduction coefficient

CONTENTS

LIST OF FIGURES

LIST OF TABLES

CHAPTER 1

INTRODUCTION

In present scenario, the lightweight alloys (Al, Mg, and Ti) have gained enormous attention because of their unique attributes such as high strength to weight ratio and ductility. Nowadays, these alloys are used extensively in every sphere from aviation, defense and aerospace to manufacturing. In the past decades, significant research and development underwent in order to develop such processes which will act as alternative to conventional severe plastic deformation methods, such as extrusion, drawing, rolling etc. These processes namely are Equal channel angular pressing (ECAE), High pressure torsion (HPT), Accumulative roll bonding (ARB). Though these processes possess significant advantages in comparison with conventional processes like; firstly, low to moderate strength, metals and alloys can be processed easily; secondly, large plastic strain (1-15) can be imposed in deformation zone; thirdly, large volume production at reasonable cost was possible. However these processes still have certain drawbacks such as multiple stages of deformation and processing of high strength metals and alloys because of the hurdles offered by tools, dies and equipment used. [1] To overcome the foresaid issues Swaminathan et al. [2] suggested a simple, low cost conventional machining process which imposed severe plastic strains in single stage of deformation during chip formation for production of ultrafine grains in forms of chips.

Though machining has become a boon among SPD processes, this process also has limitation as lack of control over shape and size of chip being formed. The geometry of the produced chip is not defined at priori in the process, so the chips produced may be curled or of limited length. To solve above problems a variant of machining process namely “large strain extrusion machining” (LSEM) was developed. Moscoso et al. [3] have investigated the production of bulk nanostructured strips by LSEM of controlled geometry in wide varieties of commercial alloys with application of different levels of shear strains imposed on chips in deformation zone. Guo et al. [4] have analyzed the deformation occurring in machining zone during LSEM using particle image velocimetry (PIV). They measured and characterized the deformation field using PIV which resulted in an intense, narrowly

confined and controllable deformation field. Iglesias et al. [5] investigated the dependency of wear rate of strips on grain size produced using LSEM process. Brown et al. [6] have studied the interactive effects of deformation field parameters and found increase in the proportion of high angle boundaries with increasing strain at small deformation rates resulted from grain refinement of materials. Sevier et al. [7] have highlighted the development of a finite element method (FEM) for prediction of deformation field parameters. It was observed that the strain produced in the chip for a given rake angle (α) was entirely controlled by chip thickness ratio (γ) [7]. The strain was seen to be uniformly distributed throughout the chip thickness with a thin primary deformation zone allowing for the application of high strain rates. Andrew Kustas et al. [8] studied the porosity level and mechanical properties of strips produced using LSEM. They discovered significant reduction in porosity, due to high shear strain and hydrostatic pressure during extrusion. Deng et al. [9-11] have investigated the thermal stability of strips using annealing heat treatment in LSEM. They found hardness as a function of annealing time and temperature [9].

Aluminum 6063 alloy which is a widely used commercially available material have many applications in architectural goods industry, rail & road transport and also in some extreme sports equipment. Because of the wide applications and lack of literature on Al6063 alloy for this process, the material was adopted so that its viability for LSEM could be verified.

1.1 Nanostructured materials

Nanostructured materials (NsM) were defined as materials made of a microstructure 100 nm-300 nm in length in at least one dimension whereas ultrafine-grained materials (UFG) possess a grain size range between 300 nm and less than 1μm in diameter. Bulk nanostructured and ultra-fine grained (UFG) metals and alloys are of extraordinary interest because of their enhanced strength properties for structural applications [1].

Nowadays most of the research interest has been largely focused on four different subject areas, processing and fabrication, characterization of material properties, microstructural characterization, and engineering design and development for new products and applications. There are several size scales that all exhibit different amounts of strengthening

based on grain size. The figure shows the terminology that corresponds to different ranges of grain size for the microstructure of fine grained materials [1].

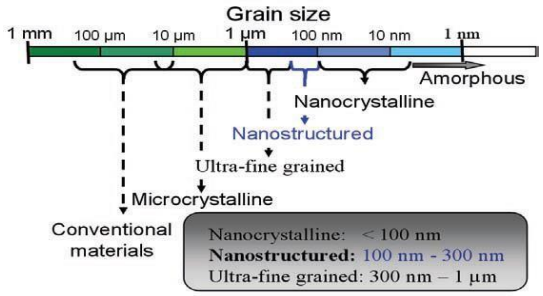

Fig 1.1 Terminology and Grain Size Ranges [2]

1.2 Properties of nanostructured materials

The most pronounced mechanical properties of nanostructured solids are high strength, hardness, ductility; and superplasticity at low temperature as compared to those of conventional coarse-grained solid materials [1].

Table 1.1 Properties of nanostructured materials

Mechanical properties	**Physical and chemical properties**
High strength	High thermal stability
High hardness	High wear resistance
Low ductility	High corrosion resistance
High superplasticity	High electrical and magnetic properties

1.3 Approaches for producing nanostructured materials

1.3.1 Top-Down approach

This approaches include the miniaturization of materials components (up to atomic level) with further self-assembly process leading to the formation of nanostructures. During selfassembly the physical forces operating at nanoscale are used to combine basic units into larger stable structures. Typical examples are quantum dot formation during epitaxial growth and formation of nanoparticles from colloidal dispersion. The biggest problem with top-down approach is the imperfection of the surface structure. Top-down approach most likely introduces internal stress, in addition to surface defects and contaminations

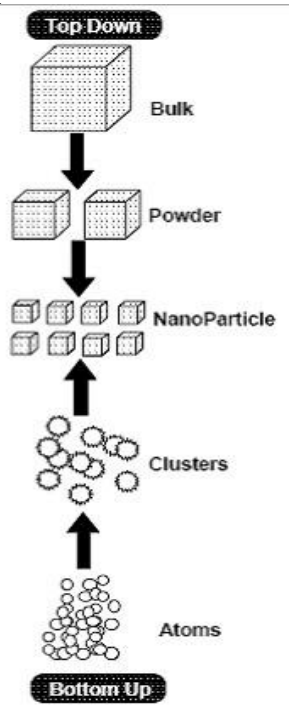

Fig 1.2 [2]

1.3.2 Bottom-Up approach

In this approach material is synthesized from atomic or molecular species via chemical reactions, allowing for the precursor particles to grow in size. Bottom-up approach also promises a better chance to obtain nanostructures with less defects, more homogeneous chemical composition, and better short and long range ordering. This is because the bottom-up approach is driven mainly by the reduction of Gibbs free energy, so that nanostructures and nanomaterials such produced are in a state closer to a thermodynamic equilibrium state.

1.4 Methods of synthesizing Nanostructured materials

There are various methods of synthesizing nanostructured materials. Some of the important methods have been shown in the table below:

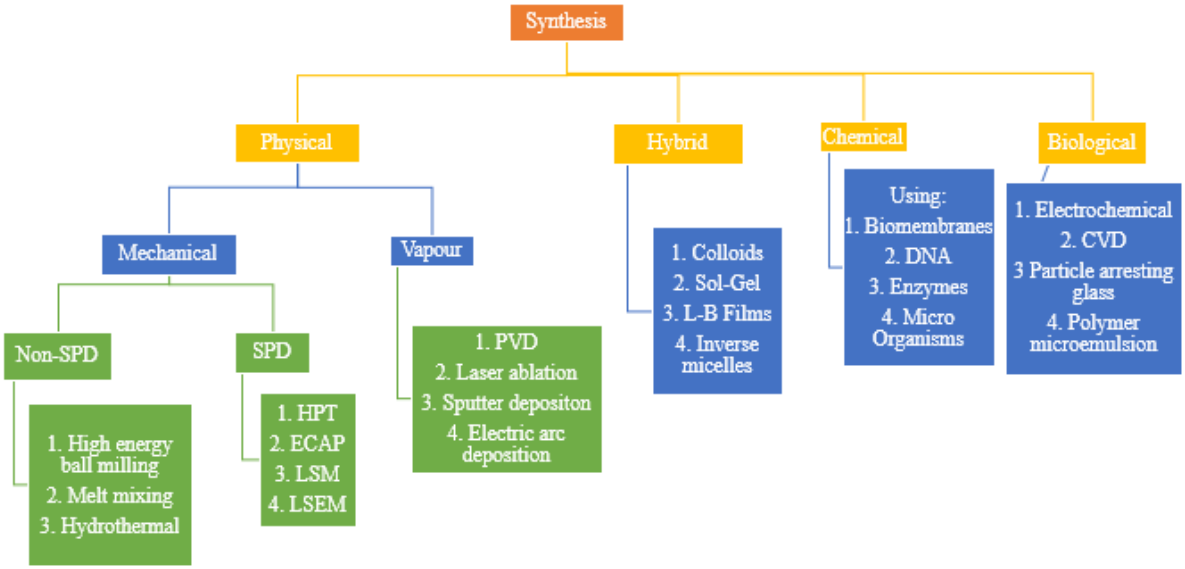

Fig 1.3 Nanostructured materials synthesizing methods [3]

1.5 Severe plastic deformation (SPD)

Severe plastic deformation (SPD) are defined as metal forming processes in which a very large plastic strain is imposed on a bulk process in order to make an ultra-fine grained metal. The objective of the SPD processes for creating ultra-fine grained metal is to produce lightweight parts by using high strength metal for the safety and reliability of micro-parts and for environmental harmony.

1.6 Different Severe Plastic deformation techniques

1.6.1 High pressure torsion (HPT)

In this technique, the sample with a diameter ranging from 10–20 mm and thickness of 0.3–0.8 mm, is placed between anvils and compressed under an applied pressure (P) of several GPa. The lower anvil turns and friction forces lead to a shear straining of the sample. To produce a homogeneous nanostructure, with a typical grain size of about 100 nm or less, deformation by several turns is necessary. Pressure plays a very important role in gaining the desired homogeneity. Among all SPD techniques, HPT has the highest grain refinement efficiency. Equivalent Von Mises strain, ε_{eq} is given by,

$$\varepsilon_{eq} = \frac{2\pi Nr}{h\sqrt{3}}, \quad (1.1)$$

Where N is the number of HPT revolutions and r and h are the radius and height (or thickness) of the disk, respectively.

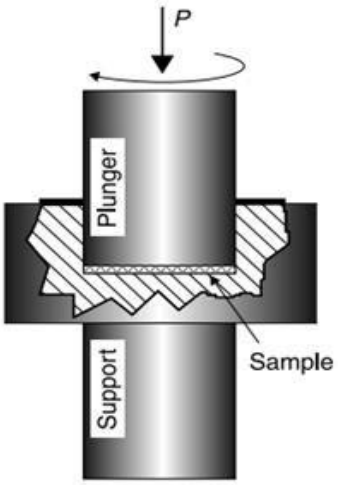

Fig 1.4 Principle of High Pressure Torsion [3]

1.6.2 Equal Channel Angular Pressing (ECAP)

In this technique, a sample of a rod or bar shape, made by compressing several thin sheets together in a die is pressed through another die constrained within a channel so that the microstructure receives shear straining leading to grain refinement to grain sizes in the submicrometer range. Each time the sheet is passed through the die, a large and homogenized strain occurs. Various routes introduce different shearing patterns into the samples leading to variations both in the macroscopic distortions of the individual grains in polycrystalline matrices and in the capability to develop a reasonably homogeneous and equiaxed ultrafine-grained microstructure.

Equal-channel angular pressing (ECAP) has attracted most attention, because it is very effective in producing UFG structures and can be used to produce UFG billets that are sufficiently large for various structural applications.

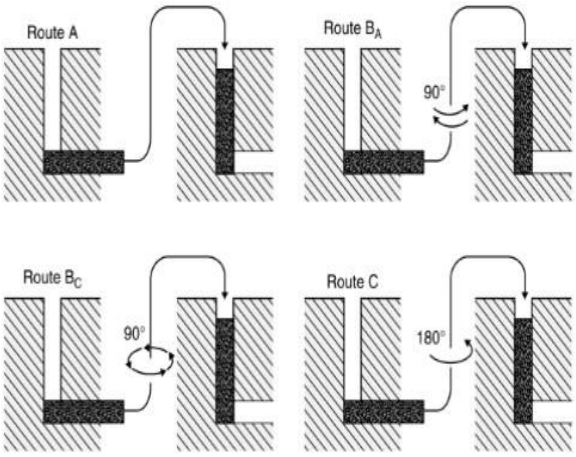

a)

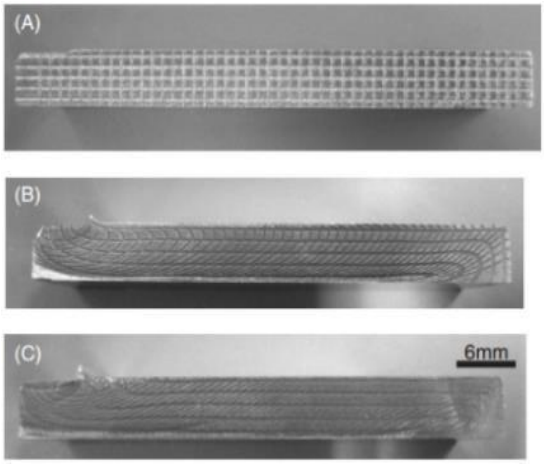

b)

Fig 1.5 a) Four processing routes of ECAP b) Observation of internal metal flow of the specimen after ECAP process. (A) Before ECAP process, (B) 1 pass, and (C) 2 passes [3]

1.7 Limitations of ECAP and HPT

1. Multiple passes of deformation are needed to reach large plastic strains using HPT & ECAP, this resulting in a degree of uncertainty in the actual deformation parameters (e.g. strain, strain rate)

2. A relatively short length of work piece that makes ECAP a discontinuous process with low production efficiency and high cost.

3. In ECAP, the ends of a work piece usually contain non-uniform microstructure or macrocracks and have to be thrown away, thus a significant portion of the work piece is wasted and the cost of the UFG materials produced by ECAP is further increased.

   The physical configurations used to realize these methods typically limit deformation to small strain rates ($<10^2\ s^{-1}$) and low deformation zone temperatures, effectively narrowing the envelope of deformation parameters that can be accessed.

1.8 Background of LSEM

The fig. illustrates LSEM process wherein material (chip) of controlled thickness and an UFG microstructure is produced by machining and extrusion imposed in a single step of deformation using a specially designed tool. In this configuration, the tool is fed in radial direction at constant feed (mm/rev) into a cylindrical shaped workpiece rotating at a constant cutting speed (V). The specially designed tool consists of two components; bottom section with a sharp cutting edge inclined at a rake angle (α) and a wedge-shaped top section made that acts as a constraining edge. Both sections are made up of a hard material. The machined material is simultaneously forced through an "extrusion" die formed by the bottom rake face and the top constraining edge, thereby, effecting dimension and shape control. LSEM can be considered a generalization of ECAE with the exemption that the thickness of the material at the tool exit can be larger or smaller than that at the inlet. This exemption ensures the imposition of levels of strain that are sufficiently high to induce formation of a refined microstructure in a single-step deformation process.

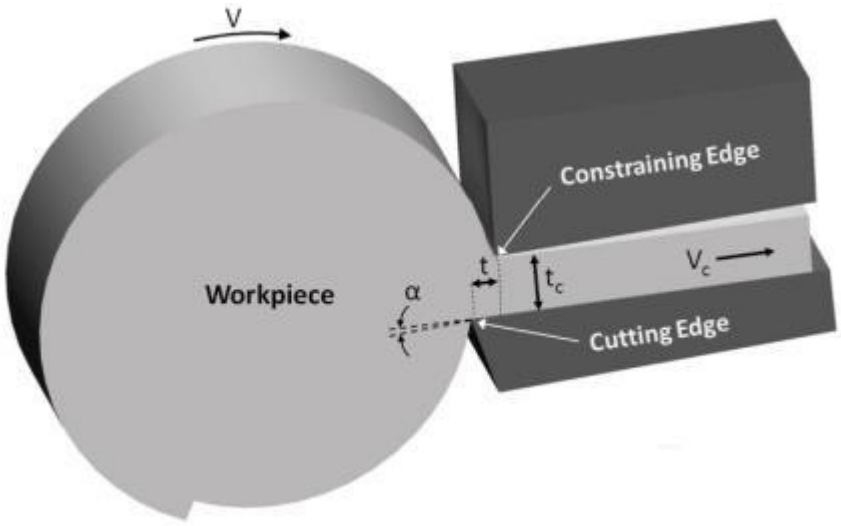

Fig 1.6 Schematic representation of LSEM [99]

1.8.1 Mathematical equations used in the study of LSEM

The shear strain imposed in plane strain LSEM due to the combined machining and extrusion depends only on the chip thickness ratio (λ) and the rake angle (α).

Various mathematical relations of metal cutting process used to calculate chip thickness ratio (λ), shear strain (γ) and other parameters are described as follows:

1. Chip reduction coefficient, $\lambda = \frac{\text{Deformed chip thickness,tc}}{Undeformed\ chip\ thickness,t}$ (1.2)

2. Shear strain, $\gamma = \frac{\lambda}{cos\alpha} + \frac{1}{\lambda cos\alpha} - 2tan\alpha$ (1.3)

CHAPTER 2

LITERATURE REVIEW

2.1 Classification of literature review on the basis of work material used:

2.1.1 BRASS

[12] L. De Chiffre (1982) discussed a new process of cutting chips from bulk and then extruding it through the gap between the constraining tool (shoe) and cutting tool. Due to this process, continuous chips with increased ductility, hardness and luster on both the faces were produced. Some of the conditions observed during experimentation in order to carry a stable process were:

1. Shoe and cutting tool edge should be sharp so that material does not collect on the cutting tool and shoe.
2. Shoe entrance angle should be 2°.
3. Feed at the start of the process should be equal to one half of gap between shoe and cutting tool and then followed by rapid increase to full feed.

Investigation was carried out and it was found that best quality chips were produced within a speed range of 60–100 m/min at $^{s}/_{h}$= 1.5, where s was gap between the shoe & cutting tool and h was distance between shoe & edge of cutting tool. Within the above stated speed range, forces were observed to be constant which is also a favorable condition for a stable process.

2.1.2 COPPER

[9] Wen Jun Deng et al. (2012) adopted Finite Element Method (FEM) to conduct experiments on pure copper to analyze advancement of temperature field, effective strain, and strain rate at distinct chip compression ratios. The cutting and thrust forces were also analyzed with respect to time.

As the value of chip compression ratio (λ) decreased, nano grained material formation was facilitated due to increases in effective strain. But at the same instant, thrust & cutting forces also increased with time at a particular values of λ and it became difficult to push the chips of the deformation zone. Results concluded from the study assured a steady LSEM process.

[10] Wen Jun Deng et al. (2013) adopted Finite Element Method (FEM) (DEFORM-2D software) to investigate and analyze the influence of constraining tool corner radius(R) on deformation behavior of pure copper and studies were conducted on structure refinement of chips in LSEM.

The effective strains and strain rates distribution were very sensitive to the constraining tool corner radius because the change in tool corner radius affects the friction at the tool chip interface which further significantly affects the effective strain associated with chip formation and hence the chip morphology. With increase in tool corner radius, a significant increase in effective strain was observed with simultaneous decrease in strain rate. Hence a wide range of ultrafine grained materials were obtained by changing the Constraining tool corner radius.

[11] Wen Jun Deng et al. (2014) adopted Finite Element Method (FEM) (DEFORM-2D software) to investigate the effect of rake angle on large strain extrusion machining and validated it with the results when the experiment on plain strain extrusion machining were conducted physically.

Simulations were done at very low speed of 0.052m/s with rake angle values varied from 5° to 30° with an increment of 5°.

Continuous chip formation was observed with chips significantly much harder and grain size smaller than the bulk material. A significant increase in cutting forces was also recorded with decrease in rake angle.

[13] S.L. Cai et al. (2015) conducted experiments on Oxygen free high conductivity (OFHC) copper on a specially designed LSEM machine. By making use of high speed imaging and digital image correlation (DIC), the detailed features of the material particle flow field in chip in LSEM were measured and a new mathematical model was developed to replicate the results of the process.

It observed that the constraining tool makes the materials moving into the shear plane to deviate from its original path by an angle (β). The angle (β) increases with the decreasing chip thickness ratio. A new equation for shear strain was developed as follows:-

$$\gamma = \frac{\lambda - sin\beta + cos\alpha tan\beta}{cos\alpha - (\lambda - sin\alpha)tan\beta} + \frac{1}{\lambda cos\alpha} - tan\alpha \qquad (2.1)$$

The maximum difference between the calculated and the observed values of chip thickness ratio ( ) and strain were about 13% and 6% respectively and was due to the tolerance of the proposed experimental setup.

Chemical composition of Oxygen free high conductivity copper(99.95%)								
Elements	Cu+Ag	Fe	S	Pb	Zn	Sn	O	Others
Wt(%)	99.97	.004	.004	.003	.003	.002	.002	.001

Fig 2.1 Chemical composition of OFHC copper

[3] W. Moscoso et al. (2007) adopted LSEM and performed a series of experiments in order to study the enhanced characteristics of nanostructured materials and ultra-fine grains (UFG) created in the form of foil, sheets, wires, rods, plates by using single pass deformation.

Data obtained from experimentation using different level of strains imposed on bulk material of OFHC copper illustrated that the hardness of nanostructured chips were significantly higher than the bulk material. TEM analysis revealed the evolution of refinement of microstructure and formation of UFG structures with increasing strain. At lower value of strain, elongated UFG microstructure were observed, while at moderate values equi-axed UFG was seen, and lastly, at highest strain, UFG of average grain diameter 250 nm was revealed.

2.1.3 ALUMINIUM

[8] Andrew Kustas et al. (2014) employed LSEM to study its practicability in eliminating porosity from a casted ingot of aluminum 5052 acquired from hydrogen entrapment during melting & casting and volumetric shrinkage during solidification.

Optical microscopy of bulk and fabricated strips was performed to compare porosity level, which was followed by Limiting Dome Height (LDH) test to compare the mechanical properties of strips produced from LSEM and conventional rolling. Optical micrographs, of the strip indicated significant porosity reduction, due to high shear strain and hydrostatic pressure during extrusion. Mechanical behavior of LSEM strips from LDH test was discovered to be ranging within conventionally rolled and annealed strips.

[2] M Ravi Shankar et al. (2005) investigated and highlighted the mechanical properties of precipitate treatable tempered alloys of aluminium. Growth of microstructure of chips in deformation zone was observed. The microstructure study suggested chips consists of equiaxed grains nearly of mean size of grains 70-100nm. The chip micro-hardness values suggested they were found to be somewhat greater than that obtained from ECAP deformation for Al6061-T6 alloy.

[11] W.J. Deng et al. (2014) studied the thermal stability of ultra-fine grains of Al alloy fabricated by LSEM. To study the thermal effects on microstructure and mechanical properties of Al alloy chips were subjected to heat treatment process called as annealing. The annealing treatments were performed at different temperatures and for different lengths of time.

Ultra-fine grains of Al alloy chips can maintain high hardness under 200°C but start losing hardness as temperature increases to 300°C and above. When annealing was done temperature less than 200°C, most of the fine grain were replaced by elongated grain there grain sizes increased with significant increase in the aspect ratio as the annealing time increased, but Vickers hardness was not reduced as expected because of precipitation of second phases.

2.1.4 MAGNESIUM

[14] Mert et al. analysed the mechanics of LSEM for deformation processing of Magnesium alloys (Mg AZ31B) for continuous production of Mg alloy sheet and foil from bulk forms in a single step of deformation applying high deformation rate and high hydrostatic pressure. Hydrostatic pressure and temperature in the deformation zone were estimated as a function of chip thickness ratio, rake angle. Capabilities to realize combinations of large strain, large hydrostatic pressure and low temperature levels, especially in a highly confined region (primary deformation zone), promoted the workability and grain refinement of alloys.

2.1.5 STEEL

[15] P. Iglesias et al. (2008) discussed new machining-based manufacturing processes with the use of which, nanostructured materials could be manufactured much economically as compared to existing methods to do so.

Shift from LSM to LSEM has been justified on PH13-8Mo Stainless steel since LSEM combines microstructure refinement by large strain machining with shape and dimensional control of the chip by extrusion, whereas in the former method only grain refinement was possible. Further a cost analysis was made considering machining cost/hour C, cutting velocity V, exit sheet (chip) thickness of t_c, chip thickness ratio □ and sheet width of w. The cost per unit volume (euros/cm3) is then,

$$Cvol = \frac{\lambda . C}{3.6 t_c w V} \tag{2.2}$$

2.1.6 LEAD

[4] Y. Guo et al. (2012) employed LSEM to study of large-strain deformation phenomena in commercially available pure lead under high level of hydrostatic pressure is applied on the shear zone. Experimentation was done under following conditions: - rake angle (α) = 10°, uncut chip thickness (h_0) = .2mm, cutting velocity (v_0) = 10mm s^{-1}, and chip thickness ratio (λ) ranging from .4 to 2.5. Rate of change of strain $\frac{d\varepsilon}{dt}$ attains its highest value at λ=1. Strain increases as the value of □ increases and further can be enhanced by reducing the shear angle value (α).

2.2 Literature summary

1. The effect of rake angle, chip compression ratio or chip thickness ratio, constraining tool corner radius and coefficient of friction on LSEM has been analyzed.

2. The formation mechanism of chips and machining parameters needed for nanostructured/ UFG strip formation in LSEM were discussed.

3. The result shows that rake angle and chip compression ratio have a significant impact on total shear strain for the strip.

4. The decrease in the rake angle causes effective strain and strain rate to be increased. But smaller the rake angle, the smaller in grain sizes the microstructure was obtained.

5. The decrease in chip thickness ratio will also cause effective strain and strain rate to be increased. But smaller the chip thickness ratio, the smaller in grain sizes the microstructure was obtained.

6. With the constraining tool corner radius or the friction coefficient increases, the strip effective strain, temperature, stress on the strip also increase, which can impact the microstructure and mechanical properties of the strip.

7. The hardness of nanostructured chips was significantly higher than the bulk material.

8. With increase in shear strain the evolution of microstructure refinement of UFG structures was found.

9. The wear rate analysis showcased that the wear rate of nanostructured material are less than microstructured material.
10. Creation of thick sheet from large strain extrusion machining was best achieved using high hydrostatic pressure or large deformation temperature.

11. The thermal stability studies, they found that UFG of Al alloy chips maintained high hardness under 200°C but started losing their hardness as temperature increases to 300°C and above.

2.3 Gaps in literature review

1. The framework to incorporate temperature effects arising at higher speeds, and rubbing induced deformation at the cutting edge. These aspects should also be facilitated by studying of a range of alloys and its process conditions,
2. The quantitative analysis of the microstructure refinement for nanostructured material has not been studied till date.
3. The mechanics of deformation for difficult to machine materials like aluminium alloys are yet not fully explored using LSEM process.
4. Corrosion resistance studies of nanostructured chips are yet to be performed.

5. The power requirements for achieving smaller grain sizes in the thicker strips have not been fully explored till date.
6. XRD analysis is yet to be performed to study microstructure refinement studies.
7. A wide range of scope lies in heat treatment studies for produces chips.

2.4 Objective of present work

1. Fabrication of nanostructured strips of Al6061T6 using LSEM under different machining conditions.
2. Detailed microstructure analysis and effect on hardness of different strips produced by LSEM.
3. To study the effect of machining parameters on shear strain induced in chips during LSEM.
4. To study deformation level changes induced in deformation zone in LSEM.

CHAPTER 3

PROCESS DETAILS OF LARGE STRAIN EXTRUSION MACHINING

3.1 Large strain extrusion machining

LSEM was done on a 2HP universal lathe with rotary configuration and specially designed tool replacing the conventional cutting tool. The tool was radially fed into the work piece rotating at an initial cutting speed of 40.47m/min with a constant feed rate of 180µm. Machining was done without the use of lubricant. Three different tools of rake angle 0°, 5° and 10° and three different cutting speeds of 40.47, 73.5 and 133.5 were used to carry out the experimentation. With continuous feeding of tool, strips of different lengths were extruded from the tool. Micro hardness testing was done using Vickers hardness tester at a load of 100gm/mm^2 with a loading time of 20 sec. Metallographic preparation was done by polishing with abrasive papers of SiC with grit size of 200. 600, 1000, 2000 followed by diamond paste polishing. XRD analysis was performed on XPERT-PRO diffractometer equipped with Cu-Kα radiation (λ=1.5418 Å). For EBSD analysis the sample preparation was the most crucial step because during EBSD the diffraction will occur in area of scanning only when the sample is completely grounded flat with mirror polished surface, for this purpose samples were further polishing with colloidal silica slurry then ion milling. EBSD scanning was conducted at centers and edge positions of strips using FEI Quanta 3D FEG (Field emission gun). TSL OIM software was used to find out the EBSD mapping, grain size, and misorientation distribution.

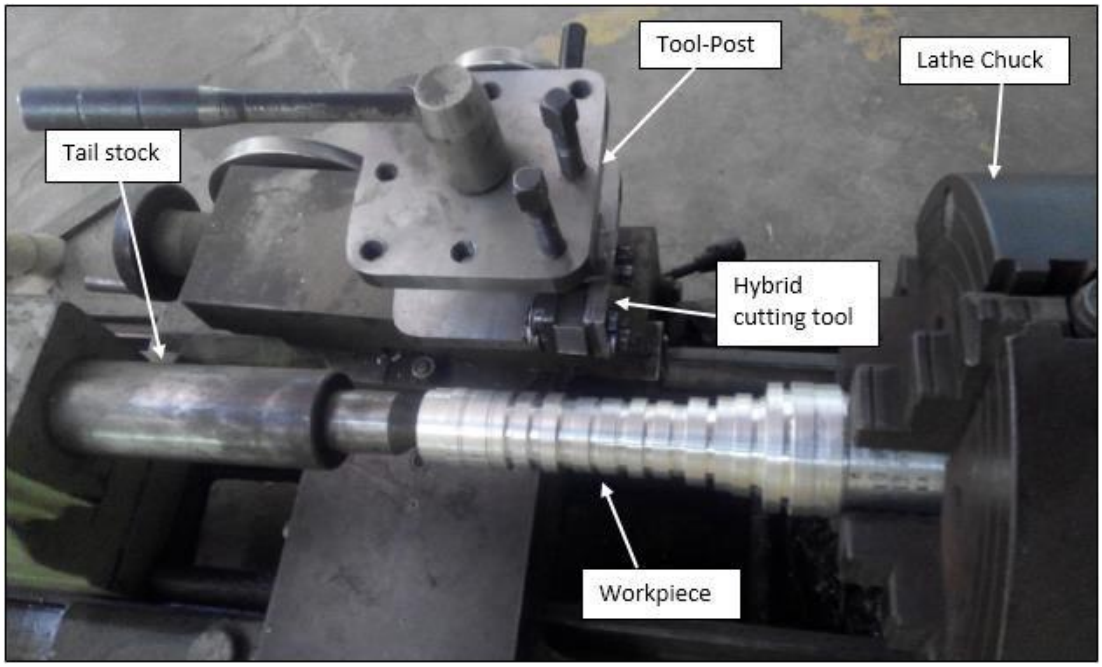

Fig 3.1 Experimental setup of LSEM

(Source: Central workshop, Thapar University, Patiala)

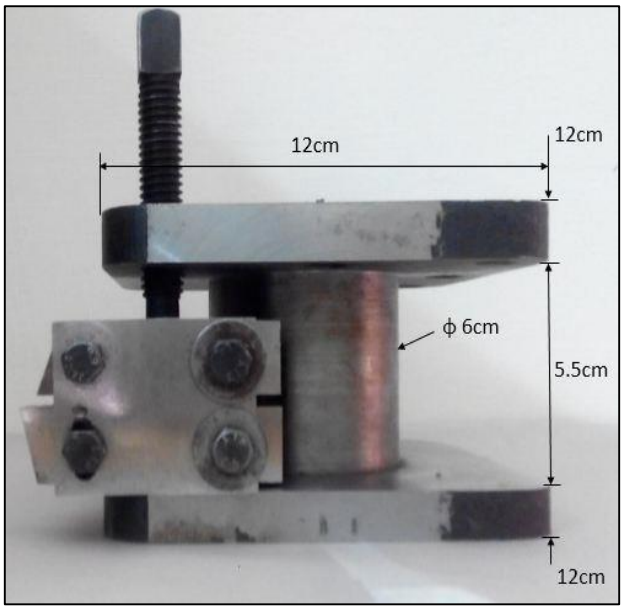

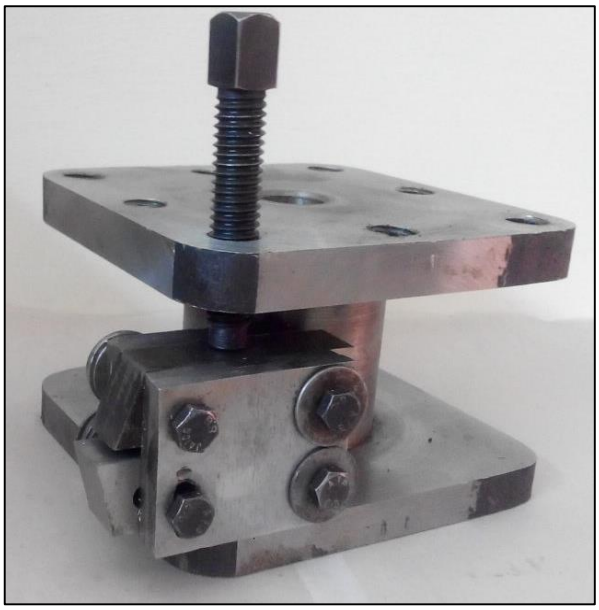

1. **2.**

Fig 3.2 Hybrid LSEM tool mounted in the tool-post (1-2)

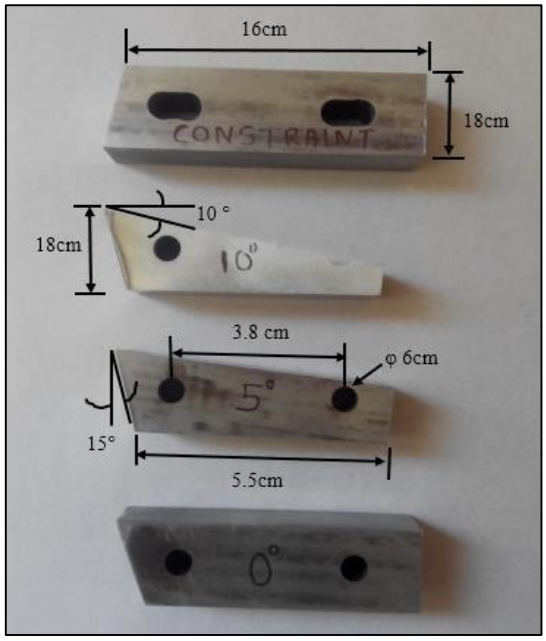

1. **2.**

Fig 3.3 Cutting tools of α= 0°, 5°, 10° and constraining tool (1-2)

CHAPTER 4

EXPERIMENTAL DETAILS AND EQUIPMENTS USED

4.1 Experimental Details

A specially designed tool was used for the fabrication of strips from commercially available Al6063. Moreover, mechanical and metallurgical characterization of bulk and strips were done to determine effect of different parameters. Cylindrical rod of Aluminium alloy with initial diameter 3 inches and length 12 inches was used for experimentation.

The cutting and constraining tools were made of high speed steel of hardness 60 HRC. This hybrid tool was an assembly of a cutting tool at the bottom and a constraining tool at the top as shown in Fig.1 and this assembly is supported by two mild steel face plates and four nut-bolts. Three cutting tools of rake angle 0°, 5° and 10° and one constraining tool were fabricated by wire EDM. The design of tool assembly is such that the desired gaps can easily be controlled.

Chemical composition of Al6063 alloy									
Elements	**Al**	**Si**	**Mg**	**Fe**	**Mn**	**Zn**	**Ti**	**Pb**	**Cu**
%	98.44	0.54	0.515	0.255	0.1	0.0418	0.0256	0.0199	0.0184

Fig 4.1 Chemical composition of Al6063 alloy

4.2 Equipment used

4.2.1 X-Ray Diffraction (XRD)

XRD analysis was performed using Panalytical X-Pert Pro diffractometer (θ - 2θ) equipped with Cu-Kα radiation (λ = 1.5418 Å). The specimens for X-ray diffraction examination were prepared by grinding with SiC papers of up to 2000 grit size to flat grounded surfaces for

performing 2-theta scanning of all samples for quantitative analysis of deformation behavior at different process conditions.

Fig 4.2 Panalytical X-Pert Pro diffractometer
(Courtesy; SAI Lab, Thapar University, Patiala)

4.2.2 Microhardness test

Microhardness analysis was done to measure the penetration resistance of the specimen. Measurements were done on a computer Interfaced Micro Hardness Tester (Model: MVH2), Meta tech industries, Pune, India available at Thapar University, Patiala. The microhardness measurement is dependent on the diameter of indentation produced on the samples. Indentation was done with a diamond cone indenter at a constant load of 100gm/mm^2 for a dwell period of 20 sec with Quantimet software. 40 MP cameras were used for observing / focusing images.

Fig 4.3 Micro Hardness Tester, Model MVH2

(Courtesy; Metallurgy Lab, Thapar University, Patiala)

4.2.3 Electron Backscatter Diffraction (EBSD)

EBSD is a microstructural or crystallographic characterization technique to study any crystalline or polycrystalline material. The technique involves understanding the structure, crystal orientation and phase of materials. Typically it is used to explore microstructures, revealing texture, defects, grain morphology and deformation.

The sample preparation for electron backscattered diffraction (EBSD) measurement is difficult and a good surface finishing is crucial. Sample preparation consisted of grinding until 2500 grit, polishing with diamond paste with size 1µm, next followed with colloidal silica slurry then ion milling.

EBSD scans were taken at their centers and near edges with a scan area of 500*500 μm^2 and step size of .5 µm, using FEI Quanta 3D FEG (Field emission gun). TSL OIM 6.1.3

software was used to find out the grain size and distribution from indexed Kikuchi patterns, grain misorientation distribution chart.

Fig 4.4 Fie Quanta 3D FEG Electron back-scatter diffraction apparatus

(Courtesy: Department of Metallurgical Engineering & Materials Science, IIT Bombay)

4.2.4 Nanoindentation

Nanoindentation is powerful technique employed to assess mechanical properties like elastic modulus, hardness, yield strength and fracture toughness of a material by making indents on its surface of load ranging in micronewtons and indentation depth in the order of nanometers. A wide range of indenters can be used depending upon the material used, property to be evaluated and type of indent. Different indenter types are berkovich, Vickers, conical/cono-spherical, cylindrical punch, knop, cube corner. [16]

In the present study TI 950 Triboindenter manufactured by HYSITRON Inc, USA has be used with a berkovich indenter of diameter 120nm, under a maximum indenter load of 1000µN. The loading, dwell and unloading time for the operation was taken to be 5sec, 2sec and 5sec respectively.

Fig 4.5 Nanomechanical Test Instrument, HYSITRON Inc, USA
(Courtesy: NanoIndentation Lab, IIT Ropar, Punjab)

4.2.5 Surface roughness tester

Surface roughness was measured using the Mitutoyo model SJ-400, Germany. The equipment uses the stylus method of measurement, has profile resolution of 12 nm and measures roughness up to 100 µm. A tracing length of 4.8 mm was used for analysis. Surface Roughness values were taken two times for each trial and average was used for analysis.

Fig. 4.6 Surface roughness tester Mitutoyo model SJ-400

(Courtesy: Metrology Lab, Thapar University, Patiala)

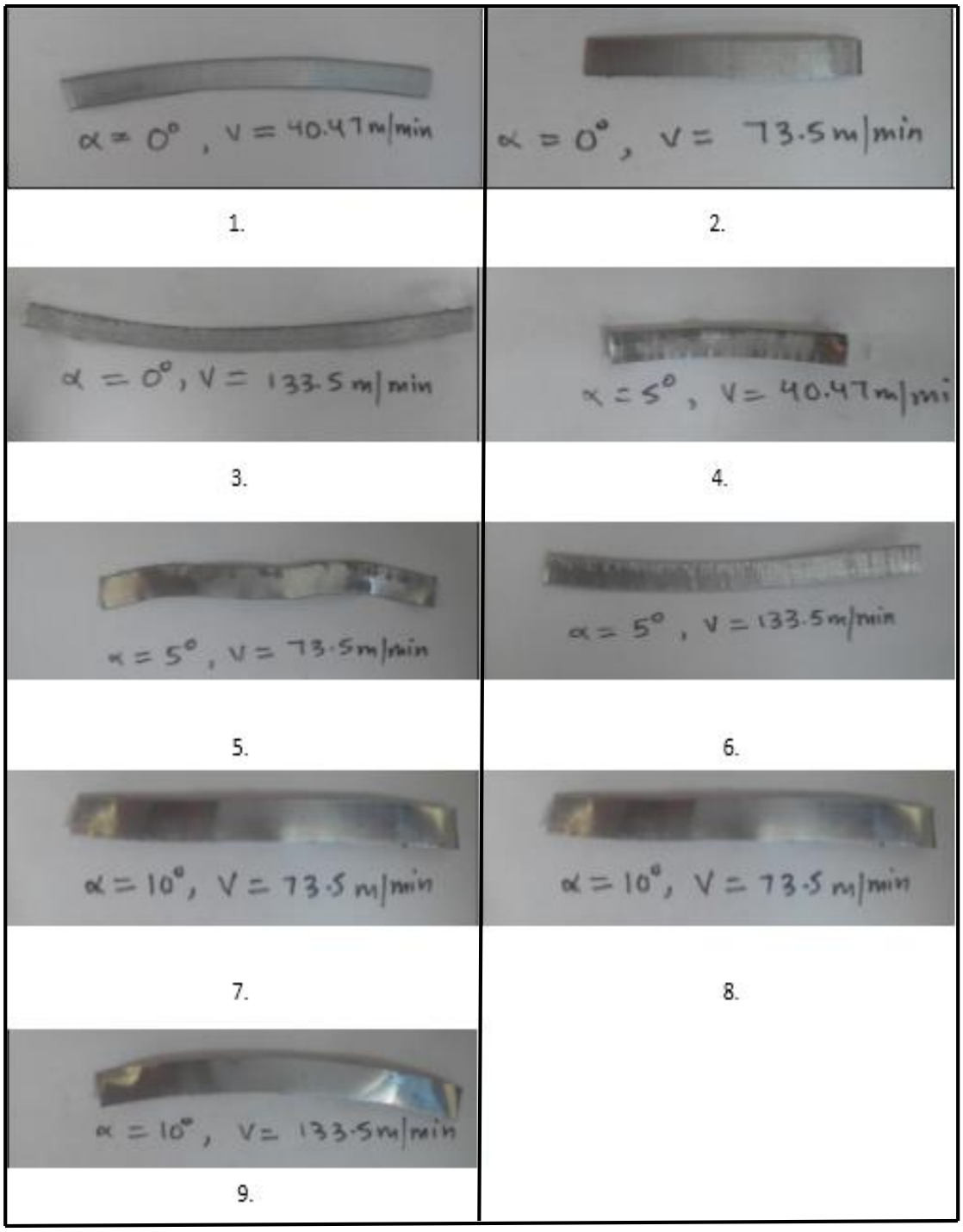

Fig. 4.7 Strips of Al6063 alloy fabricated at different machining conditions (1-9)

CHAPTER 5
RESULTS AND DISCUSSIONS

5.1 Determination of surface quality of produced strips

Surface roughness was measured using the Mitutoyo model SJ-400, Germany. The equipment uses the stylus method of measurement, has profile resolution of 12 nm and measures roughness up to 100 µm. A tracing length of 4.8 mm was used for analysis.

Table 5.1 Results of Surface roughness

Rake angle (degree)	Cutting speed (m/min)	Surface roughness (Ra)
0°	40.47	3.82
0°	73.5	2.27
0°	133.5	2.22
5°	40.47	1.71
5°	73.5	1.7
5°	133.5	1.39
10°	40.47	1.11
10°	73.5	0.96
10°	133.5	0.4

The dependency of surface roughness on cutting speed and rake angle is illustrated in Fig 5.1 Surface roughness of the samples decreases with increase in cutting speed and rake angle. The reason being, with at low cutting speeds, matrix material is deformed to a lesser extent leading to discontinuous chip formation with cracks and higher surface roughness. M. Prakash et al. [17] have studied the effect of cutting speed on surface roughness and a similar trend was observed in their investigation.

Whereas with increasing rake angle, cutting forces and power consumption reduces causing less heat generation and tool wear which further promotes continuous chip flow with reduced surface roughness.

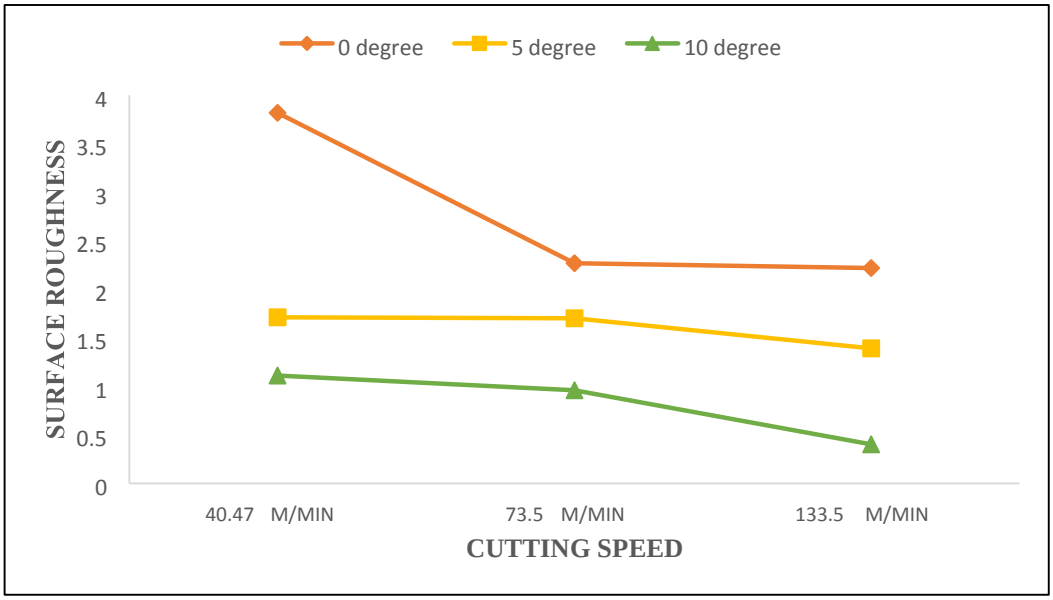

Fig 5.1 Surface roughness of machined samples at different machining conditions

5.2 Analysis of deformation level

Crystallographic deformation was studied by XRD analysis. From the XRD patterns, six most intensive reflection peaks of the samples were used in the line broadening analysis. Table 5.2 shows the value of integral breadth and full width at high maximum (FWHM) value of the peaks at specific 2θ angle for all the machined samples and bulk aluminum.

Table 5.2 Crystallite size of Al-6063 samples investigated at different machining conditions from XRD

	Position 2θ(deg)	Height (counts)	FWHM 2θ(deg)	Area (counts*2θ)	Integral breadth(area/height) β_{exp}(degree)	Crystallite size (nm)
1. Bulk Aluminum						
1	38.8465	8540.84	0.2047	2586.58	0.302	130.16
2	45.0894	5349.99	0.0895	708.85	0.132	
3	65.3426	686.8	0.1404	192.85	0.280	
4	78.4192	1416.43	0.1872	530.31	0.374	
5	82.6825	700.85	0.0936	131.2	0.187	
6	99.2128	258.43	0.1872	96.76	0.374	
2. Aluminum strips made at 0° rake and V=40.47m/min						
1	38.7912	4881.3	0.2558	1847.87	0.378	62
2	45.085	3562.85	0.1468	333.48	0.093	
3	65.3468	523.24	0.2303	178.27	0.340	
4	78.5202	1161.13	0.1092	253.59	0.218	
5	82.6191	439.57	0.307	199.68	0.454	
6	99.332	181.89	0.3744	136.2	0.748	
3. Aluminum strips made at 0° rake and V=73.5 m/min						
1	38.8303	6876.34	0.1919	1952.33	0.283	69.1
2	44.9759	4417.05	0.2175	1421.3	0.321	
3	65.6135	484.26	0.1092	105.76	0.218	
4	78.484	1483.93	0.1716	509.28	0.343	
5	82.7288	459.41	0.1872	172	0.374	
6	99.308	222.27	0.2808	124.83	0.561	
4. Aluminum strips made at 0° rake and V=133.5 m/min						
1	38.8662	4267.96	0.1716	1464.76	0.343	73.3
2	45.1845	4050.8	0.2808	2274.93	0.561	
3	65.4482	626.63	0.1404	175.96	0.280	
4	78.5832	1307.12	0.1092	285.47	0.218	

5	82.7706	461.08	0.2184	201.4	0.436	
6	99.3543	233.23	0.2184	101.87	0.436	
5. Aluminum strips made at 5° rake and V=40.47m/min						
1	38.7531	5979.52	0.2047	1810.88	0.302	82.49
2	45.0957	4226.74	0.2652	2241.86	0.530	
3	65.472	556.43	0.178	86.8	0.155	
4	78.5458	1447.12	0.1716	496.65	0.343	
5	82.7148	656.93	0.1092	143.47	0.218	
6	99.2743	228.91	0.1248	57.14	0.249	
6. Aluminum strips made at 5° rake and V=73.5 m/min						
1	38.8455	4778.37	0.1768	542.67	0.113	83.41
2	45.0333	4750.66	0.1404	1333.98	0.280	
3	65.4079	722.77	0.1716	248.06	0.343	
4	78.503	1500.09	0.156	468.03	0.312	
5	82.6967	366.14	0.1092	79.96	0.218	
6	99.2934	238.05	0.1936	44.56	0.187	
7. Aluminum strips made at 5° rake and V=133.5 m/min						
1	39.0356	3756.71	0.156	1172.09	0.311	86.37
2	45.3296	2919.97	0.1468	273.31	0.093	
3	65.605	472.69	0.178	73.74	0.156	
4	78.724	975.5	0.1404	273.92	0.280	
5	82.8795	292.37	0.1092	63.85	0.218	
6	99.4871	191.78	0.1872	71.8	0.374	
8. Aluminum strips made at 10° rake and V=40.47m/min						
1	38.8196	5929.27	0.2175	1907.9	0.321	93.17
2	45.1316	3249.41	0.156	1013.82	0.312	
3	65.4943	658.3	0.1092	143.77	0.218	
4	78.6089	1026.12	0.2496	512.24	0.499	
5	82.784	494.46	0.1092	107.99	0.218	
6	99.3545	149.61	0.1248	37.34	0.249	
9. Aluminum strips made at 10° rake and V=73.5 m/min						
1	38.8237	7898.06	0.1791	2092.92	0.264	97.13

2	44.9987	5028.23	0.2047	1522.79	0.302	
3	65.4241	764.16	0.1716	262.26	0.343	
4	78.4801	1351.44	0.1404	379.48	0.280	
5	82.7233	606.86	0.1404	170.4	0.280	
6	99.2764	244.37	0.0936	45.75	0.187	
10. Aluminum strips made at 10° rake and V= 133.5 m/min						
1	38.8456	8540.84	0.2047	2586.58	0.302	106.58
2	45.0789	5349.99	0.0895	708.85	0.13	
3	65.4026	686.8	0.1404	192.85	0.280	
4	78.5736	1416.43	0.1872	530.31	0.374	
5	82.7526	700.85	0.0936	131.2	0.187	
6	99.3526	258.43	0.1872	96.76	0.374	

From Fig 5.2 illustrates a combined comparative layout of different Bragg's peaks of XRD pattern and it can be clearly observed the presence of a single phase and no change in phase due to SPD of the machined samples. From Table 3.2 and Fig 3.2 it can be disclosed that

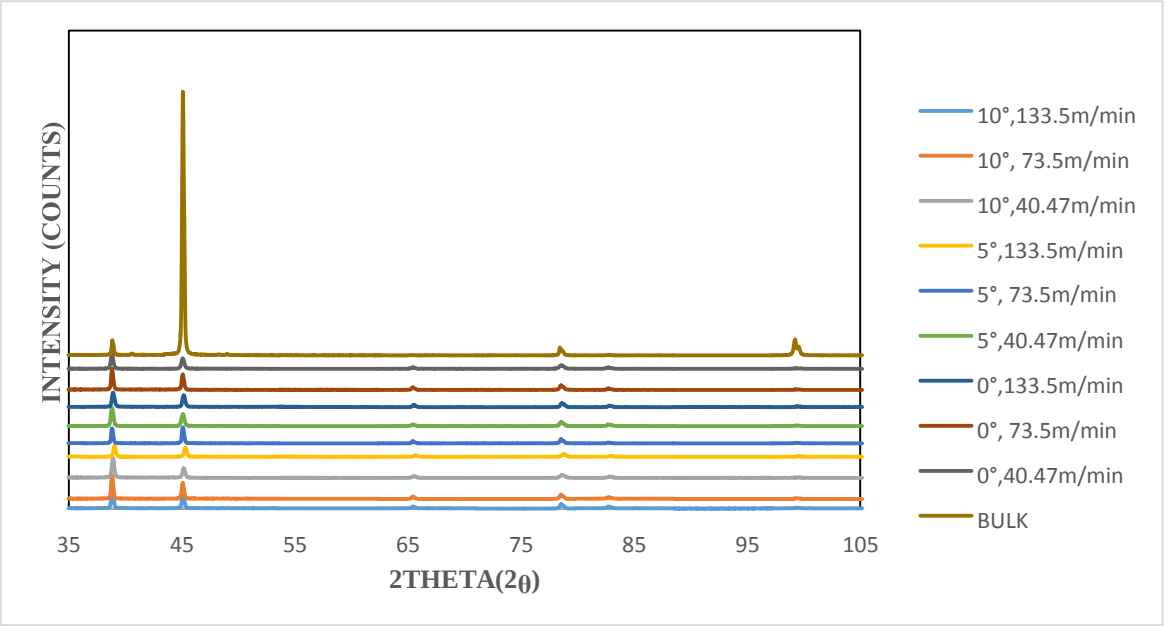

Fig 5.2 Combined graph of Bragg's peaks of XRD pattern for bulk and different machining conditions

there is broadening of XRD peaks or increasing integral breadth from bulk alloy sample to machined samples. Broadening of XRD peaks can also be observed with decrease in rake angle and decrease in cutting velocity. This broadening of XRD peaks with corresponding decrease in peak height illuminates the effect of severe plastic deformation (SPD). With XRD peaks broadening, the increasing intensity of SPD can be observed, which marks decreasing crystallite size. [18]

5.3 Analysis of Shear Strain

The variation of γ with λ at three different rakes $\alpha = 0°, 5°, 10°$ and at three different cutting speeds v = 40.47m/min, 73.5 m/min and 133.5 m/min is illustrated in Fig 5.3. There is an increase in shear strain with increase in chip reduction coefficient. The shear strain also increases with decrease in rake angle .With increase in rake angle the energy required in deformation zone reduces due to less cutting forces and less frictional heating effect. The constraint applied at point of chip formation by constraining tool controls the deformation parameters. Thus this offers us a viable opportunity to study LSEM as a severe plastic deformation process.

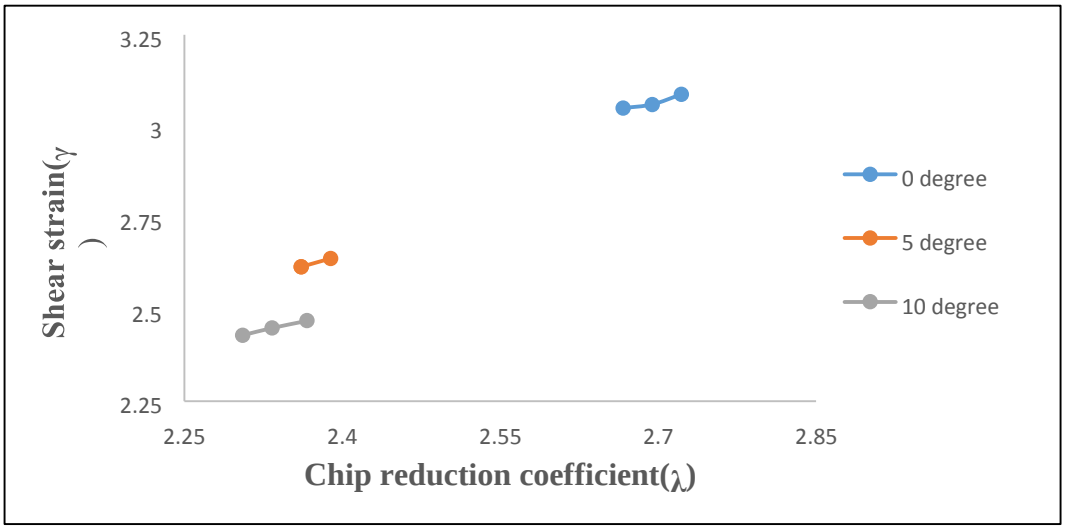

Fig 5.3 Variation of shear strain (γ) with chip reduction coefficient $\lambda = t/t_c$ at different machining conditions

5.4 Analysis of Hardness

The hardness of bulk and fabricated strips was measured on Vickers hardness tester. The results have been discussed in Table 5.3.

Table 5.3 Vickers hardness of Al6063 strips created at different level of strains

Deformation conditions	Hardness (HV)	Shear Strain (γ)
Bulk Al6063	71.51	-
α= 0°, V=40.47m/min	140.86	3.0876
α= 0°, V=73.5 m/min	111.30	3.06
α= 0°, V=133.5 m/min	104.18	3.05
α= 5°, V=40.47m/min	135.59	2.64
α= 5°, V =73.5 m/min	107.49	2.617
α= 5°, V=133.5 m/min	98.61	2.617
α= 10°, V=40.47m/min	110.3	2.47
α= 10°, V=73.5 m/min	102.1	2.45
α= 10°, V=133.5 m/min	96.81	2.43

Fig 5.4 illustrates hardness of machined samples at different machining conditions. The trend portrays reduction in hardness with increase in cutting speed and decrease in rake angle. With decrease in rake angle, forces and stresses in the PDZ increases, causing a driving force to the dislocations piled up along the grain boundaries causes low angle grain boundaries, resulting in subgrain formation or grain refinement. This grain refinement increases the dislocation density causing increased hardness of the material.

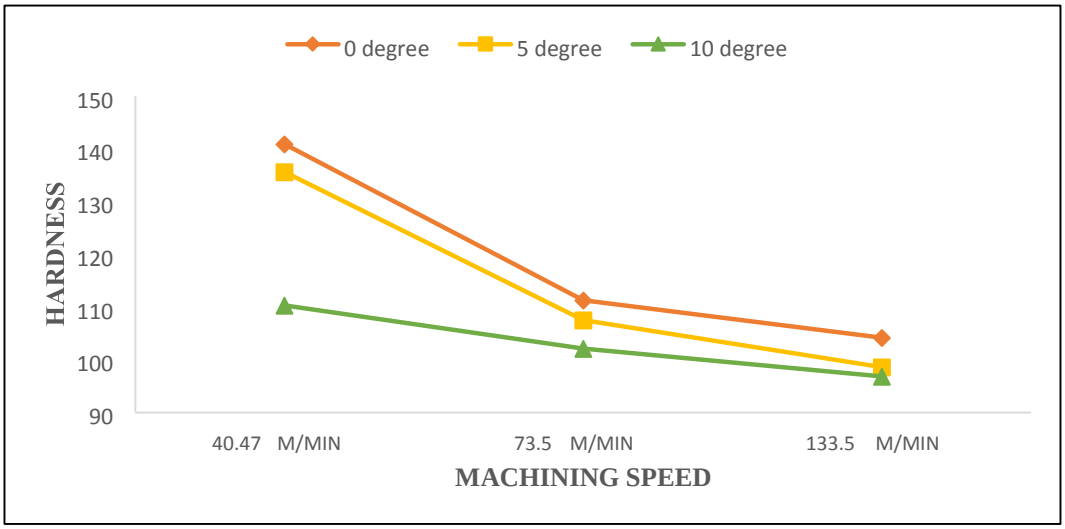

Fig 5.4 Microhardness of machined samples at different machining conditions

For a given rake angle, as the cutting speed increases temperature in the PDZ increases which promotes grain growth in the material, because of which the hardness of the material decreases. Dinakar Sagapuram et al. [19] have studied the effect of cutting speed on hardness and deformation temperature and a similar trend was observed in their study.

Fig 5.5 illustrates variation of micro hardness of samples with average crystallite size at different machining conditions. An inverse relation was observed from the trend obtained in the graph. There was a considerable increase in hardness of the fabricated strips as compared to bulk material because of grain refinement during deformation in machining zone. The amount of microstructural refinement of strips at different deformations conditions are found to be increasing with the reduction in average crystallite size of strips as compared to bulk material.

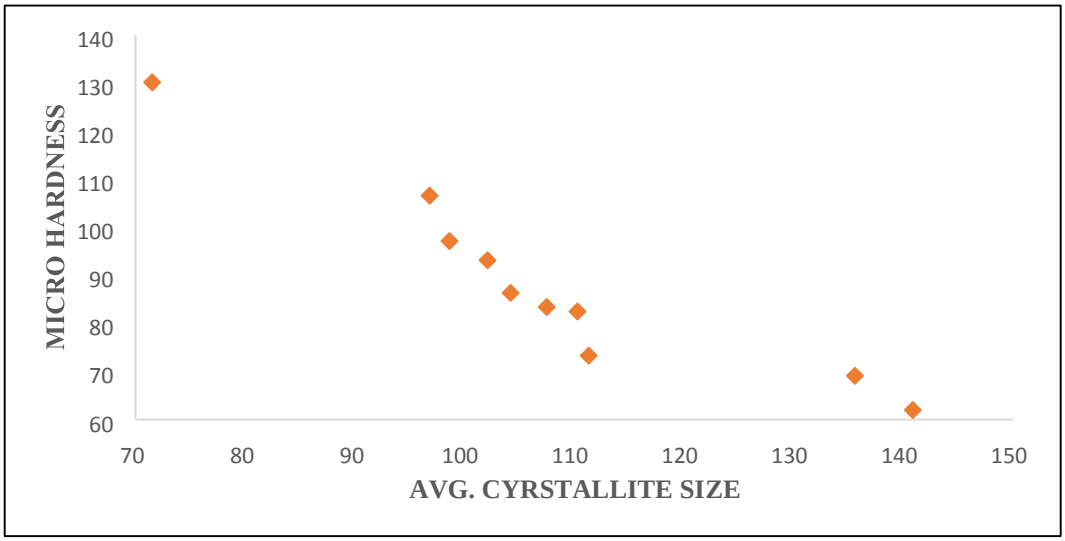

Fig 5.5 Variation of micro hardness with crystallite size

5.5 Analysis of Electron Backscatter Diffraction

5.5.1Grain Size distribution

For EBSD analysis, a square area on the surface of bulk and machined samples was scanned. For bulk sample, area of the scanned surface was selected to be 500*500mm^2 and for the machined samples, it was 100*100mm^2. It was so because the size of grains in bulk would be appreciably larger than the machined samples. So in order to optimize the scan time such conditions were adopted. EBSD map, grain size distribution and misorientation plot are shown in Table5.5. Average grain size of bulk aluminum was found to be 88.08µm with grain size ranging from .847–127.86µm. A prominent effect of SPD was spotted when the average grain size machined samples was compared to that of the bulk. Grain size had reduced to an average of 18.5 times. From the EBSD map of sample machined at 0° rake angle, grain size ranging from .165–8.97µm was observed with average grain size of 3.624µm. Due to greater level of strain, a higher density of ultra-fine grains (≤ 1 µm) were obtained. Whereas the grain size distribution plot of samples machined at 5° and 10° rake angle illustrates higher density of micro-sized grains (≥ 1 µm) with grain size ranging from .326–11.3 µm, .487–14.678µm respectively.

Table 5.4 Average grain size of Al-6063 bulk and machined samples

S. No	Sample	Average grain diameter(μm)
1.	Bulk	88.08
2.	0°, 40.47m/min	3.624
3.	5°, 40.47m/min	4.373
4.	10°,40.47m/min	6.245

From Fig 5.6 it can be observed that with increase in rake angle from 0° to 10° at a constant cutting speed of 40.47m/min, the average grain size reduced despite of the fact that the difference in the grain size was not very prominent. With increase in rake angle, easy flow of deformed material in the form of chip is facilitated due to reduction in BUE formation, cutting forces and power consumption. This combined effect leads to shear strain reduction which further leads to lesser grain refinement.

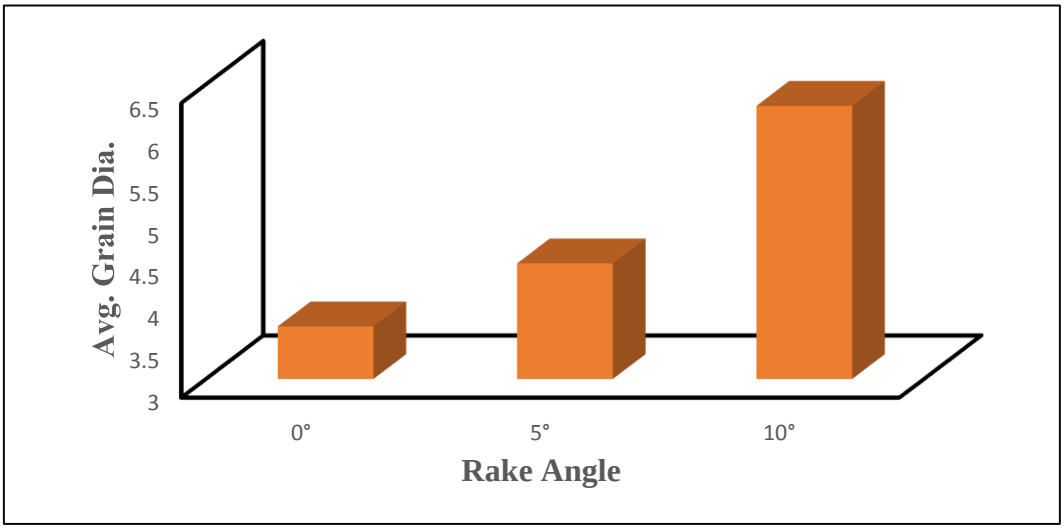

Fig 5.6 Grain size distribution of Al-6061 machined samples processed at 40.47m/min at A) 0° rake B) 5° rake and C) 10° rake

5.5.2 Grain Average Misorientation

The misorientation plot in strips illustrates the presence of large fraction of low-angle grain boundary in relation to high-angle grain boundary in bulk Al. But in machined samples at 0°, 5°, the average misorientation is 34 which signifies the presence of high angle grain boundaries because of severe plastic deformation, dynamic recystrallization leading to formation of equiaxed grains.

From the misorientation distribution it can be seen the amount of low angle grain boundaries has increased with the decrease in average misorientation of 12 in comparison with bulk aluminum by dislocation with substantial microstructural changes with shear deformation and increase in temperature due to heat generation lading to formation of elongated grains.

Table 5.5 EBSD Mapping, Grain size distribution and Misorientation plot of Bulk Al-alloy and strips fabricated at 0°, 5° and 10° rake angle at a cutting speed of 40.47m/min

Sample details	EBSD Map	Grain size distribution and Misorientation plot
Bulk		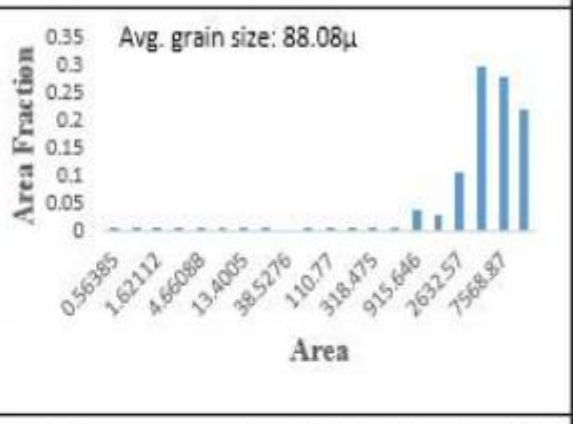
		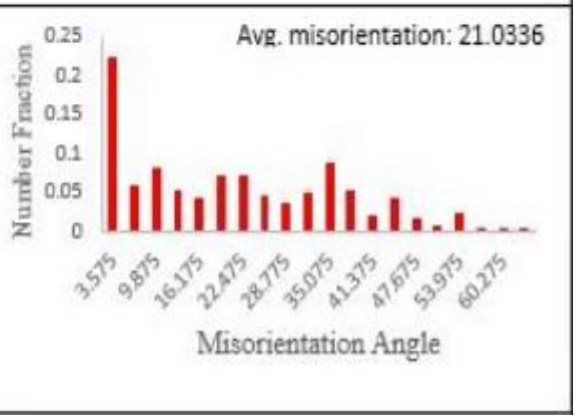

0° rake, 40.47m/min	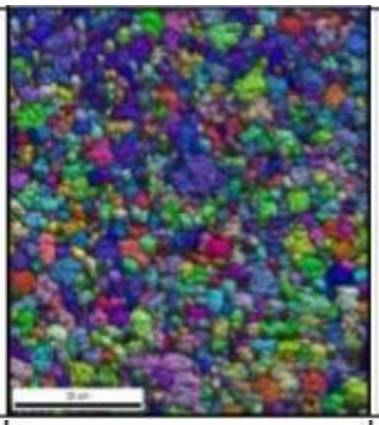	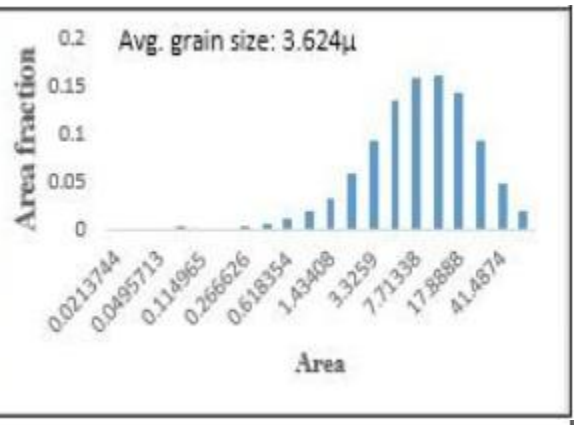
		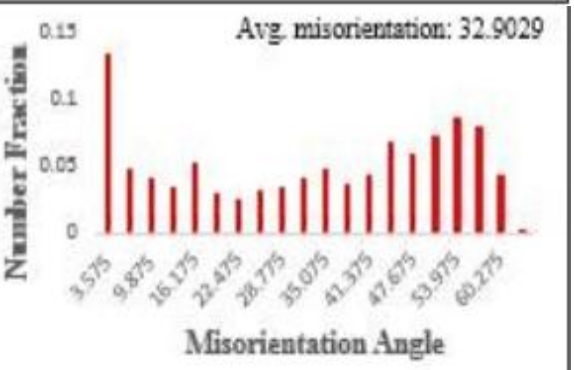
5° rake, 40.47m/min	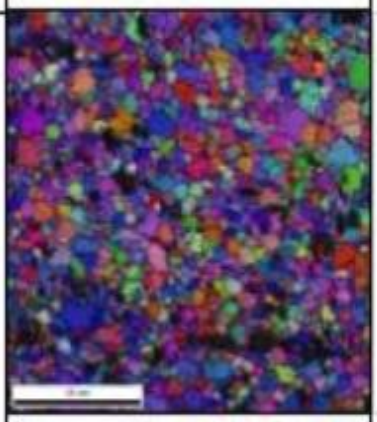	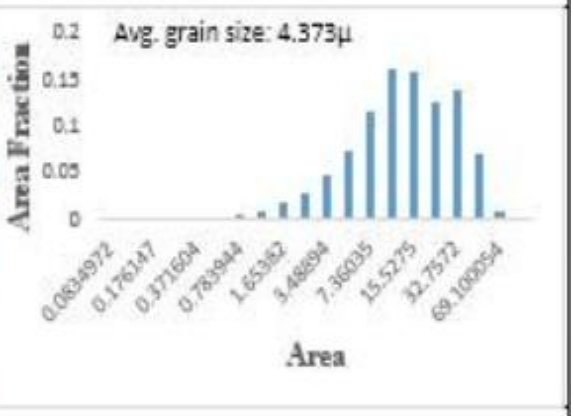
		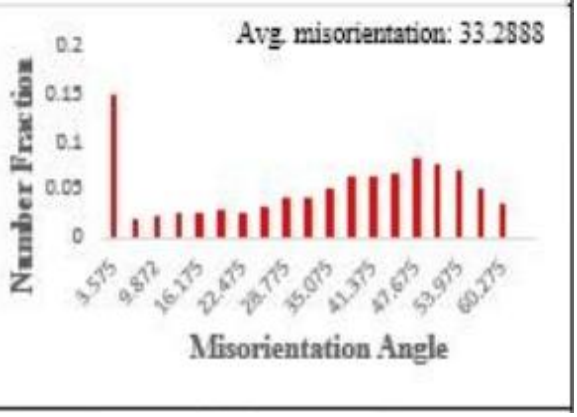

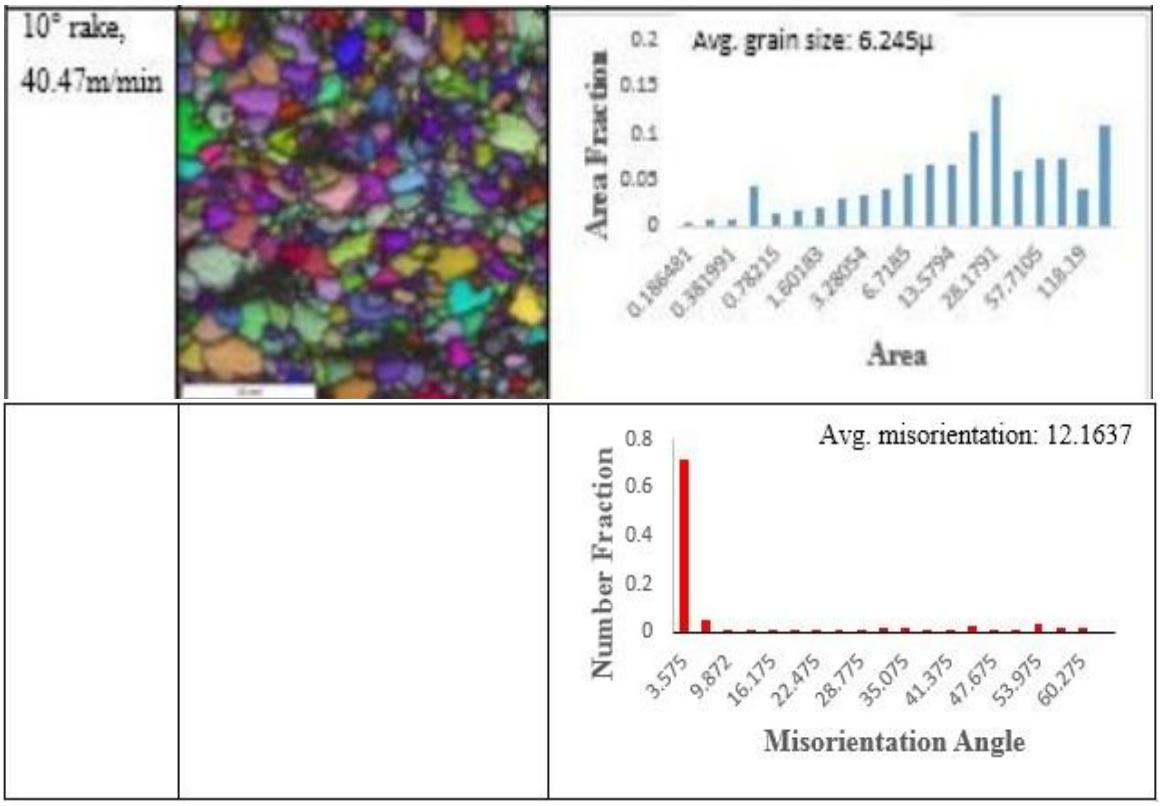

5.6 Analysis of Nanoindentation

Fig 5.7 illustrates load vs displacement curves of bulk and machined samples obtained from nanoindentation testing. Indentation was done at different locations on the samples along their lengths. Table 5.6 shows the results obtained from the testing. For nano hardness calculation of the samples, following expression was used: [20]

$$H = \frac{P_{max}}{A_c} \tag{5.1}$$

Where, P_{max} is the maximum load and A_c is true contact area. In present study, P_{max} is taken as 1000µN.

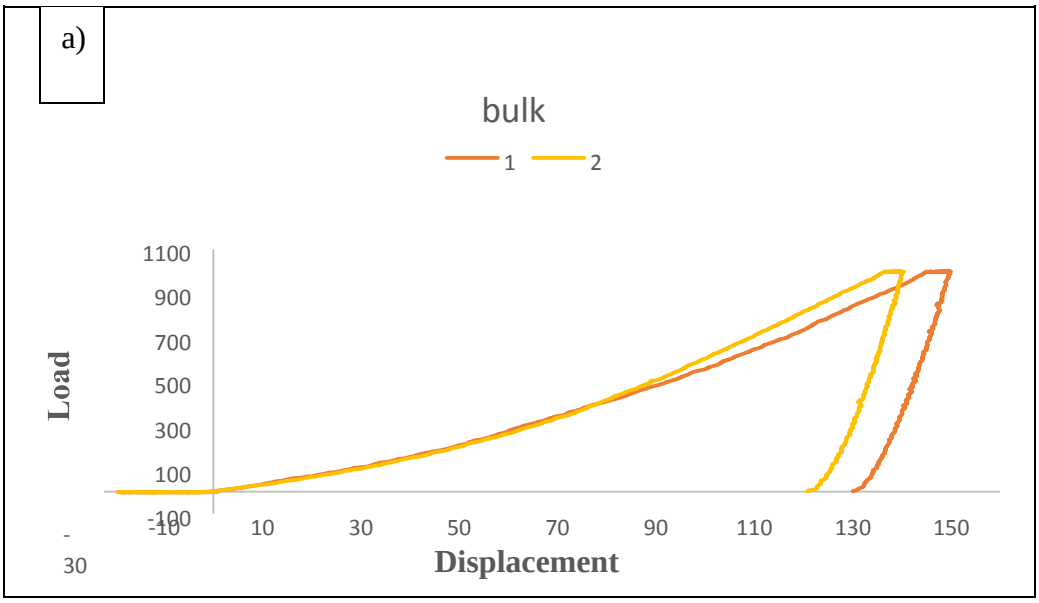
a)
bulk
1
2
1100
900
700
500
300
100
-100
Load
-30
-10
10
30
50
70
90
110
130
150
Displacement

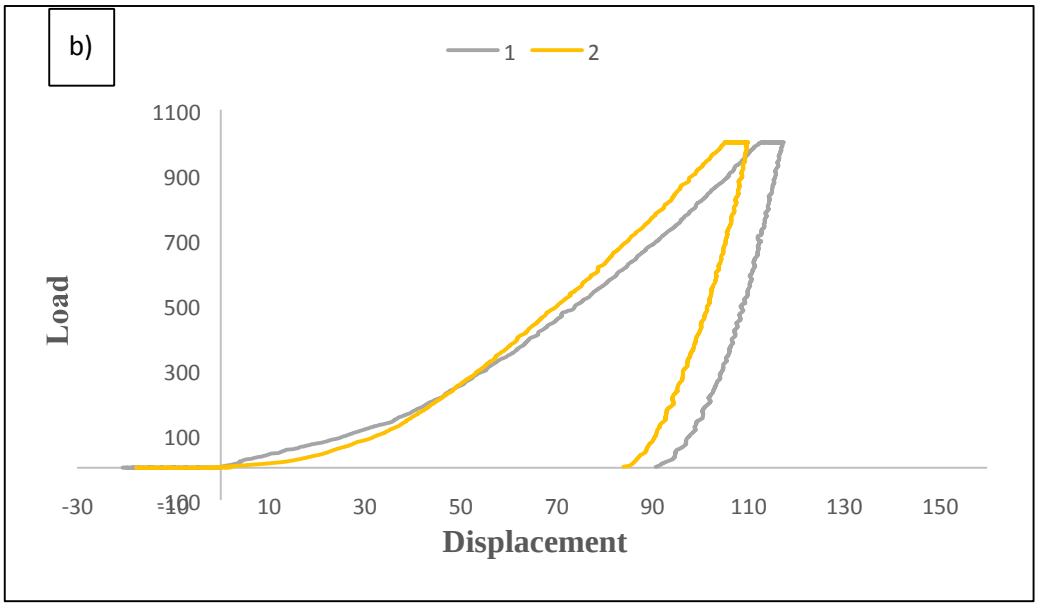
b)
1
2
1100
900
700
500
300
100
-100
Load
-30
-10
10
30
50
70
90
110
130
150
Displacement

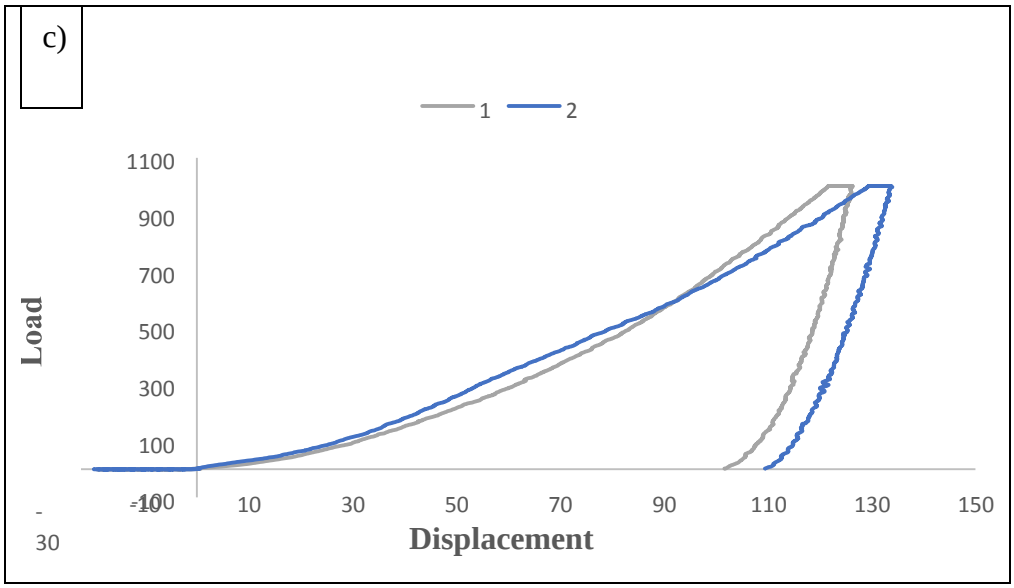

Fig 5.7 Load vs Displacement curves of a) bulk Aluminum, strips machined at b) α=0˚, 40.47m/min and c) α=0˚, 40.47m/min obtained from nanoindentation analysis.

Table 5.6 illustrates higher value of nano-hardness of machined strips as compared to bulk Al-alloy sample. Also the hardness of sample machined at 0° rake is higher than that of 5° rake sample. The average Elastic modulus of sample machined at 5° rake was also observed to be highest as compared to the other two samples.

Table 5.6 Results obtained from nanoindentation testing on bulk Al and machined samples at different rake angle values

S.NO.	Specimen	Maximum Penetration depth (h_{max})	Nanohardness (GPa)	Reduced modulus E_r (GPa)
1	Bulk Al6063 (average)	145.19	1.4	81.44
2.	Strip at α=0˚, 40.47m/min (average)	133.74	2.22	94.51
3.	Strip at α=5˚, 40.47m/min (average)	130.15	1.73	87.15

5.6.1 Strain hardening estimation

In order to estimate the extent of hardening in the bulk and machined strips, strain hardening exponent was considered. Giannakopoulos et al. [20] proposed a method with a set of equations by the help of which we could estimate strain hardening exponent (n). The equations have been enlisted below:

$$P_{max} \approx Ch_{max} \tag{5.2}$$

$$E^* = \frac{1-\nu^2}{E} - \frac{1-\nu_{in}{}^2}{E_{in}} \tag{5.3}$$

$$\frac{\sigma_{0.29}-\sigma_y}{0.29E^*} = 1 - 0.142\frac{h_r}{h_{max}} - 0.957\left\{\frac{h_r}{h_{max}}\right\}^2 \tag{5.4}$$

$$C = M_1 c\left\{1 + \frac{\sigma_y}{\sigma_{0.29}}\right\}\left\{M_2 + ln\left(\frac{E^*}{\sigma_y}\right)\right\} \tag{5.5}$$

$$\text{Strain Hardening Exponent, } n = \{\sigma_{0.29} - l(\sigma_y)\}/5 \tag{5.6}$$

Where, P_{max} = Maximum load applied, h_{max} = Maximum indentation depth, h_r = Residual depth of indentation, C = Distance from center of indent to the outer periphery of elastoplastic deformation zone, E^* = Reduced elastic modulus, ν and ν_{in} = Poisson's ratio of sample and indenter respectively, E and E_{in} = Effective elastic modulus of sample and indenter respectively. σ_y = Yield strength of indented material, $\sigma_{0.29}$ = Stress corresponding to the characteristic plastic strain of 0.29 for the indented material, M_1 and M_2 = 6.618 and -0.875 respectively for berkovich indenter.

Values of Maximum Indentation depth (h_{max}) and Residual depth of indentation (h_r) can be obtained from the load vs displacement curve. For strain hardening exponent value calculation, average of h_{max} and h_r were used. Table 5.7 portrays the values of necessary parameters for strain hardening exponent estimation and the calculated value of (n) for bulk and machined samples at different machining conditions. Value of (n) was observed to be least in the bulk sample compared to the machined samples depicting lower internal strain

which would have been acquired by the material during processing. Value of (n) was less in sample machined at 0°, as compared to that of machined at 10°.

The value of the strain hardening exponent lies between 0 and 1. A value of 0 means that a material is a perfectly plastic solid, while a value of 1 represents a 100% elastic solid. Strain hardening exponent correlate with the ability of dislocations to move around or over dislocations called cross slip. When cross slip is easy, strain hardening exponents are low. Mild steel, aluminum and Nickel alloys are some of the examples of materials that undergo slip easily. The value of (n) as cross slip becomes more difficult. Cross slip is very difficult in austenitic stainless steels, copper and brass and the strain hardening exponent for these alloys is approximately 0.5. The higher the strain hardening exponent, the greater the increase in flow stress and the greater the tendency for plastic deformation to become

Table 5.7 Parameters for strain hardening exponent estimation and calculated values of strain hardening exponent (n) for bulk and machined samples

Parameters	**Bulk Aluminum**	**Strip at α=0˚, 40.47m/min**	**Strip at α = 5˚, 40.47 m/min**
Maximum Applies load	1000	1000	1000

, P_{max}(μN)			
Residual Indentation Depth, h_c(nm)	126.27	84.02	105.53
Maximum Indentation Depth, h_{max}(nm)	145.19	133.74	130.15
h_c/h_{max}	0.869	0.628	0.810
Reduce	81.44	94.51	87.15

d Elastic Modulus, E^* (GPa)			
Effective Elastic Modulus, E(GPa)	78.12	91.4	84.05
Strain Hardening Exponent, n	0.45	0.6	0.53

uniform. Higher reduction in area can be achieved in materials with higher value of (n). For example in drawing operation, surface area of austenitic stainless steel with (n) value of 0.5 can be reduced by 50% whereas of ferritic steel with (n) value of 0.25 can be reduced only by 20 to 30%. Hence a greater Fabricability was achieved with greater strain hardening exponent. [21]

CHAPTER 6

CONCLUSIONS

1. Both cutting speed and cutting tool rake angle play a major role in controlling the strain and dimensional tolerance of the strips.
2. Hardness of the strips was found to be increased by 34-97% on grain size reduction.
3. From XRD analysis, crystallite size was found to be decreasing by 12% with increasing strain.
4. Shear strain was found to be increasing with increase in chip compression ratio and decreasing rake angle.
5. Due to strain hardening of the fabricated strips, their fabricability had increased, giving a wider scope to their applications.
6. Surface roughness of the fabricated strips was found to be improved by an average of 30% with increasing cutting velocity and rake angle.
7. Grain misorientation of some fabricated strips was found to be increasing as compared to bulk even though the grain refinement occurred in them.
8. The nanohardness of the strips was found to be greater than bulk Al6063 alloy. The change of nanohardness is strongly related to statistically stored and geometrically necessary dislocation densities.

REFERENCES

1. Sung H. Whang, Nanostructured metals and alloys- Processing, microstructure, mechanical properties and applications, *Fundamentals of aluminum metallurgy*; ISBN 978-1-84569-654.
2. Srinivasan Swaminathan, M. Ravi Shankar, Seongyl Lee, Jihong Hwang, Alexander H. King, Renae F. Kezar, Balkrishna C. Rao, Travis L. Brown, Srinivasan Chandrasekar, W. Dale Compton, Kevin P. Trumble. Large strain deformation and ultra-fine grained materials by machining Materials, *Science and Engineering A* 2005; 410–411:358–363.
3. W. Moscoso, M.R. Shankar, J.B. Mann, W.D. Compton, S. Chandrasekar, Bulk nanostructured materials by large strain extrusion machining, *Journal of Materials Research* 2007; 22:201-205.
4. Y. Guo, M. Efe, W. Moscoso, D. Sagapuram, K.P. Trumble and S. Chandrasekar. Deformation field in large-strain extrusion machining and implications for deformation processing *Scripta Materialia* 2012; 66:235–238.
5. P. Iglesias, M.D. Bermúdez, W. Moscoso, S. Chandrasekar. Influence of processing parameters on wear resistance of nanostructured OFHC copper manufactured by large strain extrusion machining, *Wear* 2010; 268:178–184.
6. Travis L. Brown, Christopher Saldana, Tejas G. Murthy, James B. Mann, Yang Guo, Larry F. Allard, Alexander H. King, W. Dale Compton, Kevin P. Trumble, Srinivasan Chandrasekar. A study of the interactive effects of strain, strain rate and temperature in severe plastic deformation of copper, *Acta Materialia* 2009; 57:5491–5500.
7. M. Sevier, H.T.Y. Yang, W. Moscoso, and S. Chandrasekar. Analysis of Severe Plastic Deformation by Large Strain Extrusion Machining, *Metallurgical and materials transactions A* 2008; 39:2645-2655.
8. Andrew Kustas, Kevin Chaput, Srinivasan Chandrasekar, Kevin Trumble. Quality of strips produced by extrusion machining directly from Cast 5052 Aluminum, *Material science and technology* 2014; 79-86.
9. Wen Jun Deng, Ping Lin, Zi Chun Xie, and Qing Li. Analysis of large-strain extrusion machining with different chip compression ratios, *Journal of Nanomaterials* 2012.

10. Wen Jun Deng, Ping Lin, Qing Li & Wei Xia. Effect of Constraining Tool Corner Radius on Large Strain Extrusion Machining, *Materials and Manufacturing Processes* 2013; 28:1090-1094.
11. Wen Jun Deng, Yong Tai He, Ping Lin, Wei Xia & Yong Tang. Investigation of the Effect of Rake Angle on Large Strain Extrusion Machining, *Materials and Manufacturing Processes* 2014; 29:621-626.
12. L. De Chiffre. Extrusion cutting of brass strips, *International Journal of Machine Tool Design and Research* 1983; 23:141-151.
13. S.L. Cai, Y. Chen, G.G. Ye, M.Q. Jiang, H.Y. Wang, L.H. Dai(2015), Characterization of the deformation field in large-strain extrusion machining, *Journal of Materials Processing Technology*, 216:48-58.
14. Mert Efe, Wilfredo Moscoso, Kevin P. Trumble, W. Dale Compton, Srinivasan Chandrasekar. Mechanics of large strain extrusion machining and application to deformation processing of magnesium alloys, *Acta Materialia* 2012; 60: 2031–2042.
15. P. Iglesias, W. Moscoso, J.B. Mann, C. Saldana, M. R. Shankar, S. Chandrasekar, W. D. Compton and K. P. Trumble. Production analysis of new machining-based deformation processes for nanostructured materials. *International Journal of material forming* 2008; 1:459–462.
16. http://ksm.fsv.cvut.cz/~nemecek/teaching/dmpo/Nemecek_nanoindentation.pdf.
17. M. Prakash, S. Shekhar, A.P. Moon, K. Mondal. Effect of machining configuration on the corrosion of mild steel, *Journal of Materials Processing Technology* 2015; 219:70–83.
18. Ravinder Singh Joshi, Sidhant Srivastava, Harpreet Singh. Microstructural analysis of nanostructured aluminum alloy strips created from machining based deformation process, 6th CIRP International Conference on High Performance Cutting, HPC2014.
19. Dinakar Sagapuram, Mert Efe, Wilfredo Moscoso, Srinivasan Chandrasekar, Kevin P. Trumble, Deformation Temperature Effects on Microstructure and Texture Evolution in High Strain Rate Extrusion-Machining of Mg-AZ31B, *Journal of Materials Science* 2012; 702-703:52-55.
20. A. E. Giannakopoulos and S. Suresh. Determination of elastoplastic properties by instrumented sharp indentation, *Scripta Materialia* 1999(10); 40:1191–1198.

21. Tensile Testing, 2nd edition. Joseph R. Davis, ASM Publisher 2014; ISBN 1615030956, 9891615030958.